Analytical Transmission Cross-coefficients for Pink Beam X-ray Microscopy Based on Compound Refractive Lenses

KEN VIDAR FALCH,[A] CARSTEN DETLEFS,[B] ANATOLY SNIGIREV,[C] AND RAGNVALD H. MATHIESEN[A,]*

[a]*Norwegian University of Science and Technology, Department of physics, Høgskoleringen 1, 7491 Trondheim, Norway*
[b]*European Synchrotron Radiation Facility, 71 Avenue des Martyrs, 38000 Grenoble, France*
[c]*Immanuel Kant Baltic Federal University, 238300 Kaliningrad, Russia*

A B S T R A C T

Analytical expressions for the transmission cross-coefficients for x-ray microscopes based on compound refractive lenses are derived based on Gaussian approximations of the source shape and energy spectrum. The effects of partial coherence, defocus, beam convergence, as well as lateral and longitudinal chromatic aberrations are accounted for and discussed. Taking the incoherent limit of the transmission cross-coefficients, a compact analytical expression for the modulation transfer function of the system is obtained, and the resulting point, line and edge spread functions are presented. Finally, analytical expressions for optimal numerical aperture, coherence ratio, and bandwidth are given.

1. Introduction

Synchrotron X-ray microscopy experiments, using X-ray optical elements to create magnified images, are typically carried out with monochromatic radiation produced by filtering the incident polychromatic beam from the source through a double-crystal monochromator, most commonly using the Si(111) reflection. This practically eliminates chromatic aberrations of refractive or diffractive optics which in turn improves the spatial resolution of the microscope, but at the cost of photon flux. The loss can be critical in experiments which require high frame rates, e.g. fast in situ X-ray imaging experiments in 2 or 3D. It is therefore of general interest to examine in detail to which extent monochromatisation can be relaxed before chromatic effects become detrimental. In the present study the transmission cross-coefficients are examined to derive compact analytical expressions for the performance of a full-field transmission microscope based on compound refractive lenses (CRLs) as function of the bandwidth of the illuminating x-rays.

The typical source for high performance X-ray microscopy at a 3rd generation synchrotron is an undulator. The undulator produces radiation with a comb-like spectrum of odd harmonic peaks. A completely non-monochromatised beam is referred to as a white beam, whereas an isolated harmonic peak commonly is referred to as a pink beam. The typical bandwidth of a harmonic peak is $\Delta E/E \sim 10^{-2}$, roughly 2 orders of magnitude larger than the typical bandwidth of a Si(111) double crystal monochromator. Both pink and white beams are used for fast lensless projection imaging [2-4], and more recently, the possibility of using compound refractive lenses (CRLs) with pink beams for focusing nanoprobes and microscopy have been demonstrated [1, 5-7].

Currently there is no simple and accurate estimate available for the modulation transfer function (MTF) of CRL-based transmission microscopes. Consequently, simple estimates for essential image forming characteristics such as point spread function (PSF), line spread function (LSF), or edge spread function (ESF) are missing. When partial coherence is to be taken into account, the straight forward integration over source points can be quite time consuming for optimization purposes, where simulations may have to be repeated when parameters are shifted. A first approximation of adding root mean square (r.m.s.) values in quadrature is sometimes used to estimate spot sizes [6-8], but this approach has a limited range of validity and can be misleading when it comes to optimization. The Hopkins method [9], sometimes also referred to as the transmission cross coefficient (TCC) method, is an effective method for simulating imaging with partial coherence. So far, direct analytical application of the Hopkins method to CRLs has not been reported.

2. Theory

Hopkins' equation is as follows [9]:

$$I(x) = \int TCC(q', q'')\tilde{F}(q')\tilde{F}(q'')^{*}\exp\left(-i(q'-q'')x\right)\mathrm{d}q'\,\mathrm{d}q''. \qquad (1)$$

Here, $I(x)$ is the image intensity, $\tilde{F}$ the Fourier transform of the complex sample transmission function, and $TCC(q', q'')$ the transmission cross-coefficients. Substituting $\overline{q} = (q'+q'')/2$, and $\Delta q = q'-q''$ allows recasting (1) into a Fourier transform with respect to Δq,

$$I(x) = \int TCC(\overline{q}, \Delta q)\tilde{F}(\overline{q}+\tfrac{1}{2}\Delta q)\tilde{F}(\overline{q}-\tfrac{1}{2}\Delta q)^{*}\exp\left(-i\Delta q x\right)\mathrm{d}\overline{q}\mathrm{d}\Delta q, \qquad (2)$$

which is convenient for numerical evaluation. In the monochromatic case, the transmission cross-coefficients are given by

$$TCC_{\text{mono}}(\overline{q},\Delta q)=\int J(q)P(\overline{q}+\tfrac{1}{2}\Delta q+q)P(\overline{q}-\tfrac{1}{2}\Delta q+q)^{*}\mathrm{d}q, \qquad (3)$$

where P is the pupil function, and J the angular source distribution. The integral in (3) must be calculated for all values of $\overline{q}$ and Δq. Fortunately, the pupil function of an x-ray CRL has the mathematically convenient Gaussian shape, even for CRLs of arbitrary length [10, 11]. Therefore,

$$P(q)=\exp\left(-\frac{q^2}{8k^2\sigma_{\text{N.A.}}^2}\right),$$

where $\sigma_{\text{N.A.}}$ is the root mean square (r.m.s.) of the transmission function of the aperture, and $k=2\pi/\lambda$, with λ as the photon wavelength. It is assumed that the pupil function is fully determined by the absorption in the CRL material, and that therefore the physical aperture is much larger than $\sigma_{\text{N.A.}}$. For typical microscopy applications, this is a good approximation [10, 12].

Furthermore the angular source distribution, as seen by the sample through any condensing optics and decoherers, is also approximated by a Gaussian,

$$J(q)=\frac{1}{\sqrt{2\pi k^2S^2\sigma_{\text{N.A.}}^2}}\exp\left(-\frac{q^2}{2k^2S^2\sigma_{\text{N.A.}}^2}\right), \qquad (4)$$

where S is the ratio between the r.m.s of the angular source distribution and $\sigma_{\text{N.A.}}$. Under these assumptions, (3) can be integrated analytically, yielding

$$TCC_{\text{mono}}(\overline{q},\Delta q)=\frac{1}{\sqrt{1+S^2}}\exp\left(-\frac{\overline{q}^2}{2k^2\sigma_{\text{N.A.}}^2\left(1+S^2\right)}-\frac{\Delta q^2}{8k^2\sigma_{\text{N.A.}}^2}\right) \qquad (5)$$

,

i.e. the TCC becomes the product of two Gaussians depending on $\overline{q}$ and Δq only.

In the above equations it has been assumed that the filtering action of the pupil function is homogenous over the field of view. This is approximately the case if the FOV is small compared to the aperture of the objective, which may not necessarily be the case for CRL microscopy. Inhomogeneous filtering gives rise to directionally dependent fringing at edges in the sample [13], but can be eliminated by focusing the illumination in the appropriate spot, g_{ideal}, downstream of the object plane. In most practical cases, this is equivalent to focusing the illumination near the objective lens plane[1]. It is possible, however, to take into account deviation from this case in the TCC formalism in order to describe other illumination schemes, such as Köehler illumination or critical ilumination. If g_{ideal} is known, any deviation between the ideal and the actual focus, g, can be simulated imposing a quadratic phase shift on the sample transmission function, F, replacing it with

$$F_{\text{foc}}=F\cdot\exp\left(\frac{ik}{2}\left[\frac{1}{g_{\text{ideal}}}-\frac{1}{g}\right]x^2\right), \qquad (6)$$

where x is the real space coordinate. In the case of a thin lens, g_{ideal} will be the distance from the sample to the objective lens position. For thick CRLs, the correct convergence of the beam can readily be calculated by means of ray tracing matrices [8, 10].

To include chromatic effects, it is necessary to integrate the intensity distribution given by (2) over the energy spectrum. The image formed by out-of-focus energies will be defocused and scaled versions of the monochromatic in-focus image. Instead of considering the bandwidth directly, it is convenient to consider the spread of defocus distances. Let $d(\alpha)$ represent the defocus distance at energy E, with $\alpha=E/E_0$ where E_0 is the in-focus energy. If the bandwidth of the pink beam is modest, $d(\alpha)$ may be linearized in terms of α as

$$d\approx\left.\frac{\partial d}{\partial\alpha}\right|_{\alpha=1}\alpha \qquad (7)$$

The power spectrum is assumed to be reasonably well represented by a Gaussian function of α, with an associated r.m.s. $\sigma_{\Delta E/E}$. Linearization of $d(\alpha)$ implies that the defocus distribution also attains a Gaussian form,

$$W(d)=\exp\left(-\frac{d^2}{2\sigma_d^2}\right), \qquad (8)$$

with r.m.s. given by

$$\sigma_d=\left.\frac{\partial d}{\partial\alpha}\right|_{\alpha=1}\sigma_{\Delta E/E_0}. \qquad (9)$$

In order to capture the effect of increased flux with increasing bandwidth, (8) have intentionally not been normalized. The full integral expression for the chromatic transfer cross coefficients is

$$TCC_{\text{ch}}(\overline{q},\Delta q)=\iint W(d-d_0)J(q)P(\overline{q}+\tfrac{1}{2}\Delta q+q)P(\overline{q}-\tfrac{1}{2}\Delta q+q)^{*}\times\exp\left(-\frac{id}{2k}\left[(\overline{q}+\tfrac{1}{2}\Delta q+q)^2-(\overline{q}-\tfrac{1}{2}\Delta q+q)^2\right]\right)\mathrm{d}q\mathrm{d}d \qquad (10)$$

Carrying out the integration over both d and q yields

$$TCC_{\text{ch}}(\overline{q},\Delta q)=\frac{\sqrt{2\pi\sigma_d^2}}{\sqrt{1+S^2+\sigma_{\text{N.A.}}^2\sigma_d^2S^2\Delta q^2}}\times\exp\left(\frac{\sum_{m,n}\overline{q}^m\Delta q^nK_{m,n}}{4k^2\left(1+S^2+\sigma_{\text{N.A.}}^2\sigma_d^2S^2\Delta q^2\right)}\right). \qquad (11)$$

The values of $K_{m,n}$ are given in Table 1. Note that only longitudinal chromatic aberration has been accounted for so far.

Lateral chromatic aberrations are related to the energy dependence of the image magnification. Similar to the case of inhomogeneous filtering, the lateral chromatic aberration can be eliminated, to the first order in d at least, by focusing the illumination in the appropriate distance g_{ch} from the sample [1]. The effect can be taken into account in the same way as the inhomogeneous filtering, i.e. by applying a quadratic phase shift to the sample transmission function,

$$F_{\text{foc}}=F\cdot\exp\left(\frac{ik}{2}\left[\frac{1}{g_{\text{ch}}}-\frac{1}{g}\right]x^2\right) \qquad (12)$$

Fortunately, g_{ch} will be equal to g_{ideal} as long as all CLR between the sample and detector planes are of one material. In most experiments involving CRLs so far, only one type of lens material is used at a time. When this is not the case it will not be possible to represent scaling and spatial filtering by (6) and (12) simultaneously, however, using $g_{\text{ch}}=g_{\text{ideal}}$ may still yield good approximations.

Table 1: Expressions for $K_{m,n}$.

Coefficient	Monochromatic term	Chromatic term	Defocus term
$K_{0,2} =$	$-(1+S^2)/2\sigma_{N.A.}^2$		$-2k^2\sigma_{N.A.}^2 S^2 d_0^2$
$K_{0,4} =$		$-S^2\sigma_d^2/2$	
$K_{1,1} =$			$-i4kd_0$
$K_{2,0} =$	$-2/\sigma_{N.A.}^2$		
$K_{2,2} =$		$-2\sigma_d^2$	

Once the expression for TCC is known, the evaluation of (2) can be performed numerically using a diagonal sum method [14]. With $\tilde{F}(q')\tilde{F}(q'')^*$ represented on a square 2D grid, and the TCCs evaluated in the grid points, integration over $\bar{q}$ can be performed by taking the diagonal sum. The remaining integral over Δq takes the form of a Fourier transform, and can be evaluated by the fast Fourier transform algorithm. An alternative method is the so-called sum over coherent systems method (SOCS)[15]. As SOCS involves singular value decomposition of the TCCs, it is not suitable for frequent re-evaluation of (2) with different parameters.

The modulation transfer function (MTF) can be calculated by going to the incoherent limit of (11), i.e. taking S to infinity. The MTF is of interest due to its simplicity and independence of $\bar{q}$. Assuming $d_0 = 0$, a relatively simple expression for the MTF can be derived, and the result is

$$\mathrm{MTF}(\Delta q) = \frac{1}{\sqrt{1+\sigma_{\mathrm{N.A.}}^2\sigma_d^2\Delta q^2}}\exp\left(-\frac{\Delta q^2}{8k^2\sigma_{\mathrm{N.A.}}^2}\right), \qquad (13)$$

when normalizing so that MTF(0)=1. The result is generalizable to two dimensions simply by replacing Δq with the magnitude of the two dimensional momentum exchange vector, $\boldsymbol{\Delta q}$. The incoherent LSF and PSF can be obtained from the MTF via numerical Fourier transformation.

Optimization

As the sample to a large extent will determine the choice of photon energy, optimization with respect to this parameter is of little general relevance, and will not be carried out here. For optimization purposes, a generic sample is chosen, represented by a small sinusoidal thickness modulation of a uniform slab. The transmission function of the sample is

$$F(x) = 1 + \varepsilon\cos(qx). \qquad (14)$$

Here q is the spatial frequency and ε the complex amplitude of the modulation. Using (14) in (2) yields an expression on the form

$$I(x) = A_0 + \mathrm{Re}(\varepsilon)A_1\cos(qx) + |\varepsilon|^2 A_2\cos(2qx) \qquad (15)$$

Assuming ε to be small, the ε^2-term can be ignored. The figure of merit to optimize is

$$\mathrm{FOM} = \varepsilon\frac{A_1}{\sqrt{A_0}}, \qquad (16)$$

and is proportional to the contrast to noise ratio (CNR). It is assumed that the noise is dominated by shot noise, and can be adequately modeled as Gaussian. The transmission function and FOM used here are chosen mainly due to the resulting mathematical simplicity, and do not necessarily represent the image quality as judged by a human observer [16]. Despite being a simple model for image quality, it captures the dependence on spatial frequency of the sample. The system also resembles one potential application of the hard x-ray pink beam microscope, namely the study of self-assembling periodic lamellar patterns in solidifying metal alloy microstructures [17]. Up to a certain point, increasing the bandwidth increases both contrast and noise, but beyond this point the noise contribution becomes dominant. In other words, there is an optimal bandwidth with respect to the CNR. The right hand side of (16) can be maximized analytically with respect to σ_d, for a given q yielding

$$\sigma_{d,\mathrm{opt}}^2 = \frac{-q^2 + \sqrt{q^4 + 16k^4\sigma_{\mathrm{N.A.}}^4 S^4\left(S^2+1\right)^2}}{4\sigma_{\mathrm{N.A.}}^4 S^4 k^2 q^2}. \qquad (17)$$

In the incoherent limit, $\sigma_{d,\,opt}$ reduces to

$$\lim_{S\to\infty}\sigma_{d,\mathrm{opt}} = \frac{1}{q\sigma_{\mathrm{N.A.}}},$$

while in n the coherent limit,

$$\lim_{S\to 0}\sigma_{d,\mathrm{opt}} = \sqrt{2}\,\frac{k}{q^2} \approx 0.11\cdot Z_T,$$

where $Z_T = 4\pi k/q^2$ is the Talbot length related to q. It should be stressed that the positive contribution of increasing σ_d stems entirely from enhanced photon flux. Increasing σ_d by enlarging $\partial d/\partial\alpha$ has no positive effect. A smaller $\partial d/\partial\alpha$ improves the CNR, regardless of bandwidth. Similarly, when considering optimization of CNR with respect to S, attention must be given to whether the total flux increases, or not. If the effective source size is determined by occlusion, increasing the source size will increase the photon flux linearly with S. In that case, the FOM should be multiplied by $S^{1/2}$ to account for it. Optimization with respect to S yields

$$S_{\mathrm{opt}}^2 = \frac{q^2 + q^6\sigma_d^4\sigma_{\mathrm{N.A.}}^4 + 2q^4\sigma_d^2\sigma_{\mathrm{N.A.}}^2 + 4k^2\sigma_{\mathrm{N.A.}}^2}{4k^2q^4\sigma_d^4\sigma_{\mathrm{N.A.}}^6 - 2q^6\sigma_d^6\sigma_{\mathrm{N.A.}}^4 - 4q^4\sigma_d^2\sigma_{\mathrm{N.A.}}^2 - 4k^2\sigma_{\mathrm{N.A.}}^2 - 2q^2} + \frac{q^2\sqrt{q^4k^8\left(1+\left(q^8\sigma_d^8+16k^4\sigma_d^4\right)\sigma_{\mathrm{N.A.}}^8 + 4q^6\sigma_{\mathrm{N.A.}}^6\sigma_d^6 + 6q^4\sigma_{\mathrm{N.A.}}^4\sigma_d^4 + 4q^2\sigma_{\mathrm{N.A.}}^2\sigma_d^2\right)}}{4k^2q^4\sigma_d^4\sigma_{\mathrm{N.A.}}^6 - 2q^6\sigma_d^6\sigma_{\mathrm{N.A.}}^4 - 4q^4\sigma_d^2\sigma_{\mathrm{N.A.}}^2 - 4k^2\sigma_{\mathrm{N.A.}}^2 - 2q^2} \qquad (18)$$

In the case where the illumination intensity remains constant while the angular source changes, the optimal S is

$$S_{\mathrm{opt}}^2 = \frac{q^2 - 4k^2\sigma_d^2\sigma_{\mathrm{N.A.}}^4 + q^4\sigma_d^2\sigma_{\mathrm{N.A.}}^2 - 4k^2\sigma_{\mathrm{N.A.}}^2}{4k^2\sigma_{\mathrm{N.A.}}^2\left(1+\sigma_{\mathrm{N.A.}}^2\sigma_d^2q^2\right)} + \frac{q^2\sqrt{1+\left(16k^4\sigma_{\mathrm{N.A.}}^8 + q^4\sigma_{\mathrm{N.A.}}^4\right)\sigma_d^4 + 2q^2\sigma_d^2\sigma_{\mathrm{N.A.}}^2}}{4k^2\sigma_{\mathrm{N.A.}}^2\left(1+\sigma_{\mathrm{N.A.}}^2\sigma_d^2q^2\right)} \qquad (19)$$

The expression for the optimal numerical aperture is impractically large, and has been included as supplementary material. Fortunately, optimization of the MTF yields

$$\sigma_{\mathrm{N.A.,\,opt}}^2 = \frac{q^2}{8k^2} + \frac{\sqrt{q^4\sigma_d^2 + 16k^2}}{8\sigma_d k^2}, \qquad (20)$$

which is a much more compact and agreeable expression.

3. Results and discussion

Figure 1 shows the LSF and PSF calculated for the pink beam case by using (13), together with the monochromatic case were the PSF and LSF are identical. Evidently and perhaps not surprisingly, the chromatic spread functions have tails, and those of the LSF are more severe than for the PSF.

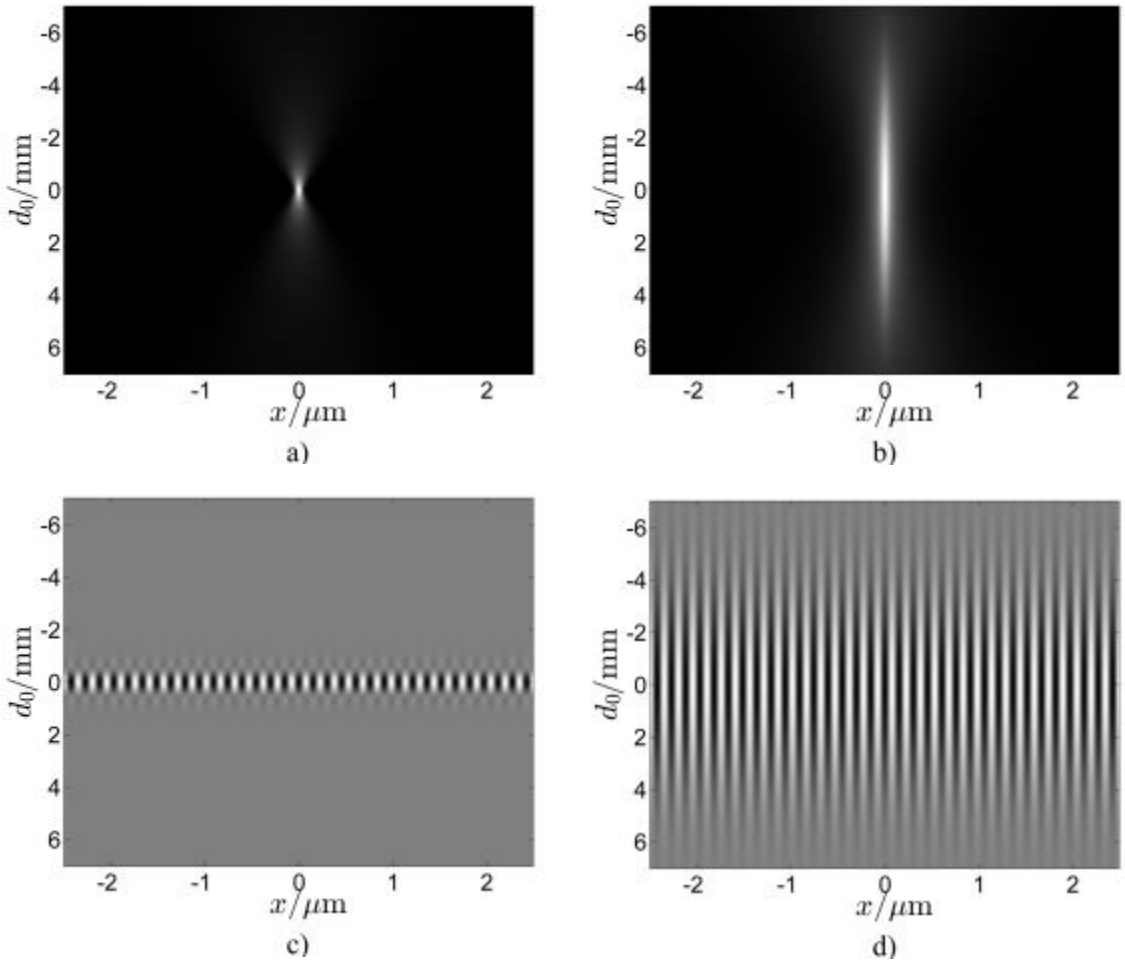

Figure 2: Simulated 1D images at different defocus d_0. (a) and (b) are monochromatic and pink beam images, respectively, of a Gaussian with 10 nm r.m.s. value, which is small compared to the diffraction limit of 75 nm. (c) and (d) are monochromatic and pink beam images, respectively, of a grating with period of 150 nm. A coherence ratio of S=0.5 was used in the simulations. The other parameters used were E_0=35keV, and $\sigma_{N.A.} = 1.05 \cdot 10^{-4}$. In the pink beam case, σ_d=2.55 mm was used, while σ_d=0 was used in the monochromatic case.

In the monochromatic case, adding a third line (equally spaced) makes little contribution to the contrast between the first two, provided that they are separated by a distance comparable to the diffraction limit. In the pink beam case, however, the presence of additional lines can make significant contributions to contrast between the other two. The sinusoidal sample model used here assumes an infinite periodic sample and will therefore take into consideration the long tail of the LSF.

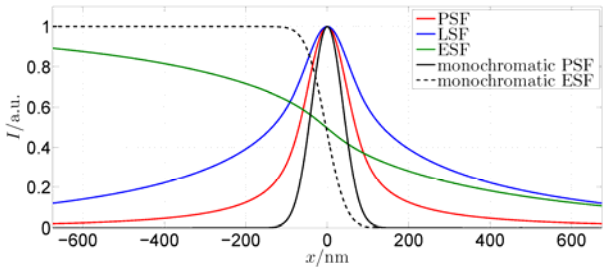

Figure 1: The LSF and PSFs for the pink beam and monochromatic beam cases. The LSF is determined by an inverse Fourier transform of the 1D MTF, and a slice of the PSF has been extracted by applying the Fourier slice theorem to the 2D MTF. The ESFs were calculated by convoluting the LSF with a step function. The parameters used in the calculation were σ_d=5.4 mm and $\sigma_{N.A.}$=1.5·10^{-4}.

Figure 2 compares 1D images of two Gaussian shaped objects at different defocus lengths. Depth of field (DOF) with monochromatic illumination is mostly a matter of numerical aperture. It is evident that with pink-beam illumination, σ_d can come into play in a significant manner as well. A coherence ratio of 0.5 was used to create the images in Figure 2. It should

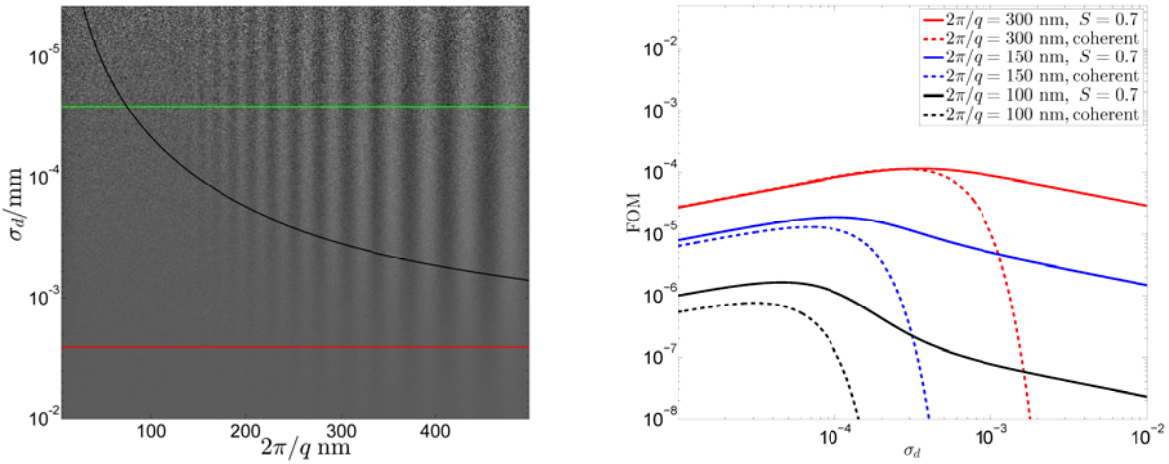

Figure 3: a) Simulated 1D images with noise, computed for different bandwidths. The black line indicates the optimal bandwidth as given by (17). The green and red curves indicate Si-111 monochromatic and pink beam case, respectively, with rate of defocus at $\partial d/\partial \alpha = 0.6$. *The monochromatic bandwidth was set to* 10^{-4} *(FWHM), and the pink beam bandwidth was set to* 10^{-2} *(FWHM). The figure appearances depend on several parameters choices, where the most decisive ones are* $E_0 = 17$*keV,* $S = 0.5$, *and* $\sigma_{N.A.} = 1.75$, *corresponding to a diffraction limit of 93nm.*

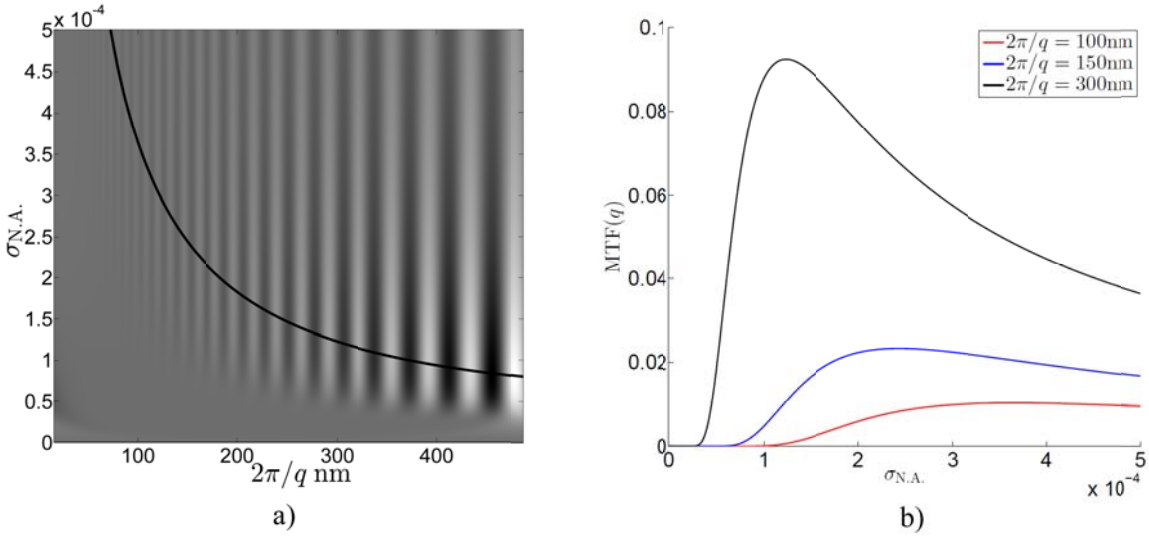

Figure 4: (a) Simulated 1D images of a sinusoidal wave with gradually changing period. The simulation is based on the MTF. Each horizontal line is an individual image, simulated with different N.A.. The horizontal axis is labeled with the length of the period. The black line indicates the N.A. that optimizes MTF(q), according to (20). Parameters used were E = 17 keV, $\sigma_d = 2.5$ *mm. (b) MTF as a function of* $\sigma_{N.A.}$ *at different values of q.*

be noted that in (c) and (d), such an increase in DOF is not achieved when a highly coherent beam is used, due to emergence of interference patterns.

Figure 3 illustrates the effect of varying σ_d. Artificial noise was added to Figure 3 a) to capture the detrimental effect of low flux. Although optimizing FOM does not necessarily optimize the image quality as judged by a human observer, it seems to come rather close in this case. Increasing the bandwidth beyond the optimal is of course detrimental to the resolution, but it should be noted that the DOF at the optimal bandwidth is comparable to the monochromatic DOF. Significant gain only occurs when σ_d is increased beyond the optimal. Figure 3 b) shows the FOM for three different values of q, with $S = 0.7$, and with perfect coherence. Both the perfectly coherent and partially coherent curves starts off with an incline proportional to $\sigma_d^{1/2}$, which suggests that the exposure time required to reach a given CNR is proportional to σ_d, as should be expected. In the coherent case there is a rather sharp cutoff near the optimum, where FOM declines rapidly, while with a partial coherence, the descent is much slower.

Figure 4 shows simulated 1D image with varying N.A.. It is evident that there is quite a bit of contrast to be gained by optimizing the aperture to a specific spatial frequency.

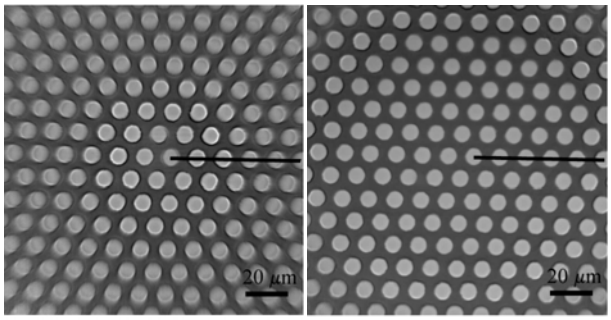

Figure 5: Experimental images of a copper mesh from a previously published experiment [1]. (a) and (b) were recorded with parallel illumination and with converging illumination, respectively. The convergence was due to a condenser lens configured to focus the source inside the objective. The exposure time was 6 ms in both cases.

The theory and optimization presented here is concerned with perfect lenses. Real CRLs, of course, have aberrations that will influence the image quality. Figure 5 shows two images taken from a previously published experiment [1], using 17.1 keV photon energy, recorded with an objective and condenser consisting of 84 and 32 double concave 50 μm apex radius Be lenslets, respectively. The condenser was positioned to focus the illumination into the center of the objective, and a beam decoherer, which produced a coherence length of ~150nm[18] corresponding to S≈0.6, was placed approximately 10 cm downstream of the condenser. The sample was a 4 μm thick Copper mesh and was placed 300 mm upstream of the objective lens. The distance from the objective lens to the detector was 2600 mm. Figure 6 compares simulations based on the presented theory to the experimental results sampled from the black lines in Figure 5. The defocus in the simulations was set to $d_0 = 4.6$ based on an estimate that considered the apparent difference in magnification of the experimental curves [1].

There is a notable mismatch between the simulation and the experimental data, the most significant of which is the exaggerated contrast in the simulation presented in a). In b) there is a reasonable agreement that gets progressively worse towards the periphery of the FOV, i.e. as x increases. It is notable, however, that in the region between 15-30 μm, the agreement is quite good, especially considering that the simulation parameters were simply taken from estimates, without parameter fitting. The fit is somewhat better when using *g=-30 cm*, which corresponds to regarding the decoherer as the effective source plane.

While it is tempting to attribute the improvement to the decoherer, it cannot be ruled out that spherical aberrations might be the real cause. Spherical aberration in the type of lenses that were used in the experiment, namely 50 μm apex radius Be lenses, have been reported [6, 19]. If spherical aberration was present, it would, in the parallel beam case, produce a defocused image by an amount that differs over the FOV. Figure 7 shows the same simulations as in Figure 6, repeated with $d_0 = -4$ mm. The x = 15-30 μm region is no longer a good fit, however the x=0-10 μm region is now in much better agreement than in Figure 6. Furthermore, the contrast level in the focused beam simulation is close to that of the experiment, albeit with some new fringe features. It should be mentioned that the appearance of fringes is rather sensitive to the choice of S. The contrast level largely depends on the transmission of rays representing low spatial frequencies, which in the focused beam case travel mostly through the center the lens where spherical aberration is least prominent. This might suggest that the defocus that gives a good fit in the center of the FOV would also give a better estimate of the contrast. Thus spherical aberrations seem to be an important source of discrepancy between the simulations and

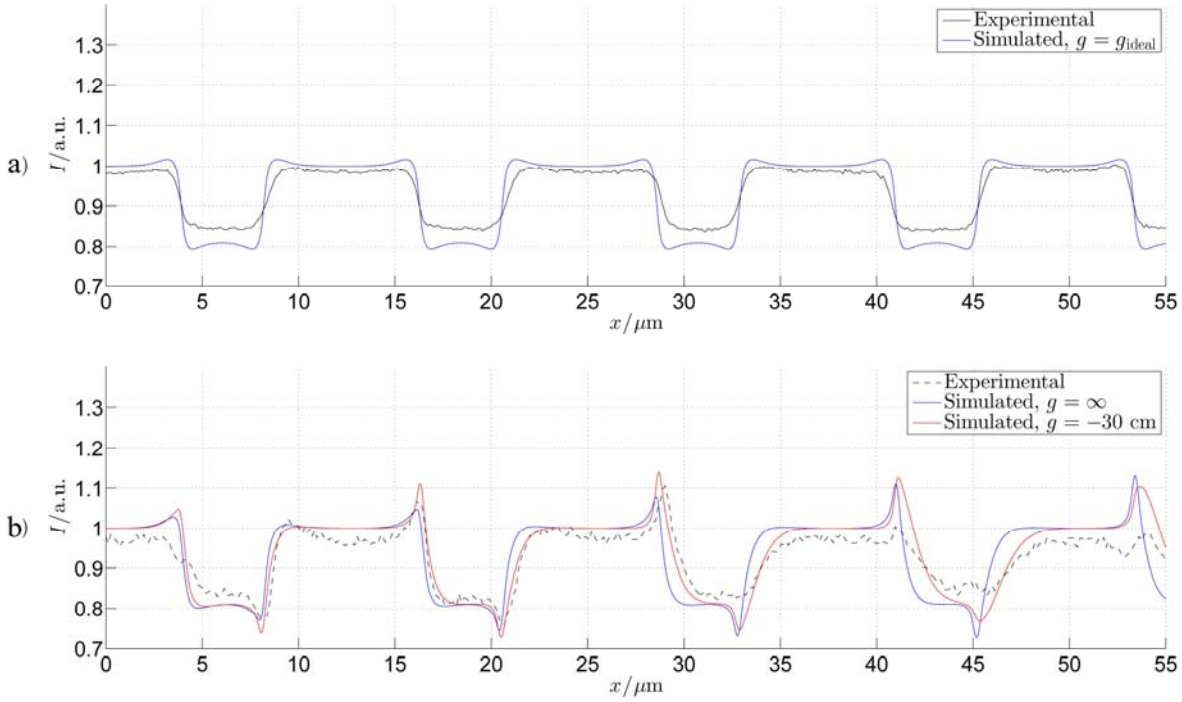

Figure 6: Comparison with experimental results [1]. x=0 is in the center of the FOV. a) Beam focused into objective. b) Parallel beam illumination. Note that g is the only parameter that was changed in the simulations. All other parameters were the same for all three simulations. d_0 was set to 4.6 mm, as estimated in [1, 2] . Other parameters used were σ_d = 3.6 mm, $\sigma_{N.A.} = 1.75 \cdot 10^{-4}$, E = 17 keV, S = 0.7, and g_{ideal} = 30 cm. The curves were flat field corrected with a simulated featureless sample, to compensate for vignetting of the FOV.

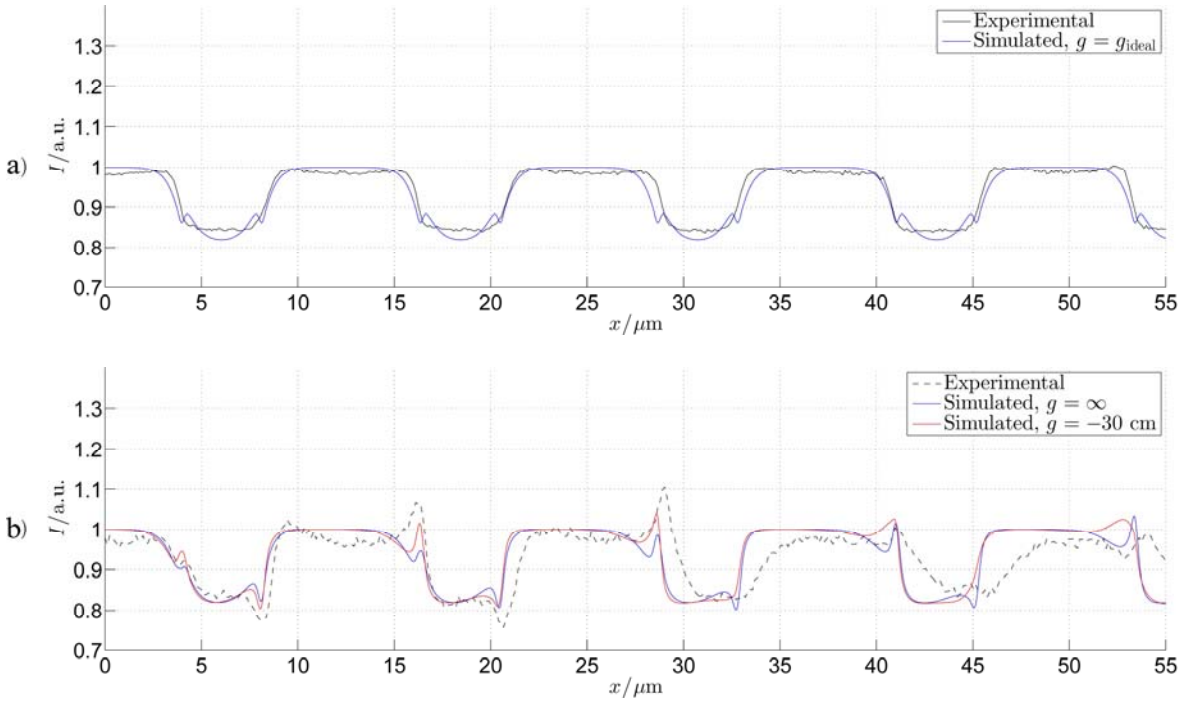

Figure 7: Comparison with experimental results [1]. x= 0 is in the center of the FOV. a) Beam focused into objective. b) Parallel beam illumination. d_0 was set to -4 mm, which yields an improved fit near x = 0 and a closer agreement with the experimental contrast levels. All other parameters were the same for all three simulations, and were identical to those used in Figure 6.

experiments.

4. Conclusion

The transmission cross-coefficients for an x-ray microscope based on compound refractive lenses were derived using Gaussian approximations of the source shape and energy spectrum. The effects of partial coherence, defocus, beam convergence, as well as lateral and longitudinal chromatic aberration are included in the solution. An analytical expression for the MTF was obtained, as well as for optimal numerical aperture, coherence ratio, and bandwidth. Comparison with experimental data shows qualitative agreement, however, it is likely that a more detailed model of illumination or lens aberrations, or both have to be taken into account in order to produce better simulations. It might be interesting to compare our results with a full scale 2D image simulation based on the synchrotron radiation workshop (SRW)[20], which is currently the most developed software package for x-ray optics simulations. SRW supports inclusion of defects and apertures. It might be interesting to investigate to what degree these results are valid when aberrations and apertures are included.

References

1. Falch, K.V., et al., *Correcting lateral chromatic aberrations in non-monochromatic X-ray microscopy.* Applied Physics Letters, 2016. **109**(5): p. 054103.
2. Ludwig, O., et al., *In-situ three-dimensional microstructural investigation of solidification of an Al-Cu alloy by ultrafast x-ray microtomography.* Metallurgical and Materials Transactions A, 2005. **36**(6): p. 1515-1523.
3. You, J.X., et al., *Interfacial undercooling in solidification of colloidal suspensions: analyses with quantitative measurements.* Scientific Reports, 2016. **6**: p. 28434.
4. Rack, A., et al., *Exploiting coherence for real-time studies by single-bunch imaging.* Journal of Synchrotron Radiation, 2014. **21**: p. 815-818.
5. Falch, K.V., et al., *In situ hard X-ray transmission microscopy for material science.* Journal of Materials Science(accepted, unpublished), 2016.
6. Seiboth, F., et al., *Focusing XFEL SASE pulses by rotationally parabolic refractive x-ray lenses.* 22nd International Congress on X-Ray Optics and Microanalysis, 2014. **499**.
7. Dufresne, E.M., et al., *Pink-beam focusing with a one-dimensional compound refractive lens.* Journal of Synchrotron Radiation, 2016. **23**: p. 1082-1086.
8. Falch, K.V., et al., *Zernike phase contrast in high-energy x-ray transmission microscopy based on refractive optics.* Ultramicroscopy, 2016. **Under Review**.
9. Hopkins, H.H., *On the Diffraction Theory of Optical Images.* Proceedings of the Royal Society of London Series a-Mathematical and Physical Sciences, 1953. **217**(1130): p. 408-432.
10. Simons, H., et al., *Full-field hard x-ray microscopy with interdigitated silicon lenses.* Optics Communications, 2016. **359**: p. 460-464.
11. Kohn, V.G., *Semianalytical Theory of Focusing Synchrotron Radiation by an Arbitrary System of Parabolic Refracting Lenses and the Problem of Nano-Focusing.* Journal of Surface Investigation-X-Ray Synchrotron and Neutron Techniques, 2009. **3**(3): p. 358-364.
12. Snigireva, I., G.B.M. Vaughan, and A. Snigirev, *High-Energy Nanoscale-Resolution X-ray Microscopy Based on Refractive Optics on a Long Beamline.* 10th International Conference on X-Ray Microscopy, 2011. **1365**: p. 188-191.
13. Schroer, C.G., et al., *Beryllium parabolic refractive x-ray lenses.* Design and Microfabrication of Novel X-Ray Optics, 2002. **4783**: p. 10-18.
14. Yamazoe, K., *Fast fine-pixel aerial image calculation in partially coherent imaging by matrix representation of modified Hopkins equation.* Applied Optics, 2010. **49**(20): p. 3909-3915.
15. Saleh, B.E.A. and M. Rabbani, *Simulation of Partially Coherent Imagery in the Space and Frequency Domains and by Modal Expansion.* Applied Optics, 1982. **21**(15): p. 2770-2777.

16. Burgess, A.E., *The Rose model, revisited.* Journal of the Optical Society of America a-Optics Image Science and Vision, 1999. **16**(3): p. 633-646.
17. Witusiewicz, V.T., et al., *The Ag-Al-Cu system - Part I: Reassessment of the constituent binaries on the basis of new experimental data.* Journal of Alloys and Compounds, 2004. **385**(1-2): p. 133-143.
18. Falch, K.V., *High-energy X-ray Transmission Microscopy based on Compound Refractive Lenses*, in *High-energy X-ray Transmission Microscopy based on Compound Refractive Lenses*. 2017, Norwegian University of Science and Technology. p. 40-44.
19. Koch, F.J., et al., *Quantitative characterization of X-ray lenses from two fabrication techniques with grating interferometry.* Optics Express, 2016. **24**(9): p. 9168-9177.
20. Chubar, O., et al., *Development of Partially-Coherent Wavefront Propagation Simulation Methods for 3rd and 4th Generation Synchrotron Radiation Sources.* Advances in Computational Methods for X-Ray Optics Ii, 2011. **8141**.